Geomechanics and Engineering, *Vol. 8, No. 2 (2015) 257-282*
DOI: http://dx.doi.org/10.12989/gae.2015.8.2.257

Transient analysis of monopile foundations partially embedded in liquefied soil

Amin Barari [1], Mehdi Bayat [*1], Meysam Saadati [2],
Lars Bo Ibsen [1] and Lars Andersen Vabbersgaard [1]

[1] *Department of Civil Engineering, Aalborg University, Sohngårdsholmsvej 57, 9000 Aalborg, Aalborg, Denmark*
[2] *Department of Civil Engineering, Babol University of Technology, Babol, Iran*

(*Received October 20, 2014, Revised October 07, 2014, Accepted November 17, 2014*)

Abstract. In this study, the authors present a coupled fluid-structures-seabed interaction analysis of a monopile type of wind turbine foundations in liquefiable soils. A two dimensional analysis is performed with a nonlinear stiffness degradation model incorporated in the finite difference program Fast Lagrangian Analysis of Continua (FLAC), which captured the fundamental mechanisms of the monopiles in saturated granular soil. The effects of inertia and the kinematic flow of soil are investigated separately, to highlight the importance of considering the combined effect of these phenomena on the seismic design of offshore monopiles. Different seismic loads, such as those experienced in the Kobe, Santa Cruz, Loma Prieta, Kocaeli, and Morgan Hill earthquakes, are analyzed. The pore water pressure development, relative displacements, soil skeleton deformation and monopile bending moment are obtained for different predominant frequencies and peak accelerations. The findings are verified with results in the liter.

Keywords: offshore monopile; liquefaction; inertia effect; dynamic response; numerical analysis

1. Introduction

Offshore wind farms are becoming increasingly popular in the quest for renewable sources of energy. There have been strong political and industrial pressures to enlarge the Danish Offshore Wind Energy sector by up to 3000 MWs. Various foundation solutions can be used for offshore wind-energy converters, including monopiles, gravity and tripod foundations, and bucket foundations (Achmus *et al*. 2009, Sørensen and Ibsen 2013, Li *et al*. 2011, Barari and Ibsen 2012, Ibsen *et al*. 2012, 2014). As one option for wind turbines, the offshore monopile foundation consists of a large-diameter steel pile that transfers the static and dynamic loads into the seabed.

The offshore environment is introducing new challenges to wind turbine technology and many of these challenges have not been addressed properly from the technical- economic standpoint (Breton and Moe 2009). The cyclic loading, caused by the interaction of the wind turbine with waves and winds or due to strong ground motion, causes the accumulation of displacements on the foundations during the operational lifetime of a wind turbine (Depina *et al*. 2013). It is therefore necessary to consider lateral response of monopile foundations as a major concern for offshore and

*Corresponding author, Ph.D. Student, E-mail: meb@civil.aau.dk; bayat.me@gmail.com

http://www.techno-press.org/?journal=gae&subpage=7 ISSN: 2005-307X (Print), 2092-6219 (Online)

earthquake engineers, by the design of monopile foundation to ensure the serviceability of offshore wind energy converters.

Current design codes for deriving the static and lateral capacity of monopile foundations rely on the American Petroleum Industry (API) method also known as *p-y* curves method. Due to the absence of soil continuum effects and the fact that deformations are not directly linked to the number of load cycles in API methodology, numerical simulations with nonlinear material models are preferably used in the analysis of the laterally loaded monopiles.

Finite element analyses were utilized to study the influence of cyclic loading conditions on the rate of pore pressure accumulation. For example, Taşan *et al*. (2010) reported the results of two-phase finite element based on porous media using a hypoplastic constitutive model for sand due to cyclic loading of large-diameter monopile. The response of monopile was calculated by steady state analysis and the quantitative determination of pore water pressure accumulation close to the monopile. They showed that the pile behavior is highly affected by pore water pressure accumulation around the shaft. Lesny and Hinz (2007) and Achmus *et al*. (2009) combined long-term cyclic triaxial tests with numerical method relating the reduction of the soil secant stiffness to the load cycles, stress state and empirical coefficients derived from cyclic triaxial tests.

The researchers have also performed some tests on small scale single piles, to take the effects of soil density and pile installation into account, although their applicability to large-diameter monopiles under long-term cyclic loadings are uncertain (Long and Vanneste 1994, Lin and Liao 1999).

The analysis and design of pile foundations in seismically liquefiable soils have drawn considerable attention in recent years, due to the reported case histories of some earthquakes (Bhattacharya 2006, Haldar *et al*. 2008, Haldar and Babu 2010).

As one of the most important and complex phenomena in geotechnical earthquake engineering, liquefaction contributes heavily to the severe damages of facilities due to the complex inertial and kinematic interactions between piled foundations and the surrounding soil (Tokimatsu *et al*. 1996, Tokimatsu and Asaka 1998, Lin *et al*. 2005). In most major earthquakes (i.e., Alaska 1964, Niigata 1964, Loma Prieta 1989, and Kobe 1995), lateral soil spreading and large ground displacements affect bridges, buried pipelines, and structure foundations (Hamada 1992, Ishihara 1993, Bhattacharya *et al*. 2005). Failure modes in offshore pile foundations subjected to extreme and cyclic loadings were investigated by Ryu and Yun (1992) based on the results of the dynamic analysis using the first-excursion probability analysis. Butterfield and Gottardi (1996) presented the failure of offshore foundation based on a system of parabola and rotated ellipses. Jiang *et al*. (2011) presented different failure modes for pile which supported by sleeve when it is subjected to static and cyclic load. Wang *et al*. (2013a) employed finite element method to present the soil wedge failure on both sides of offshore monopile foundation under monotonic loading while multi-layer soils were considered. Later, Wang *et al*. (2013b) studied the failure patterns of monopile foundation for offshore wind turbine under various combinations of load components by using three-dimensional finite element method.

Very few works in the existing literature on offshore monopiles have examined seismic design in the context of inertia and the kinematic forces arising from the deformation of the surrounding soil. In this paper, the authors investigate an axisymmetric circular monopile offshore foundation subjected to seismic loads. Five different seismic excitations are considered for a monopile founded in two-layer soil deposits. The finite difference method (FDM) is used in the Fast Lagrangian Analysis of Continua (FLAC) software code to obtain dynamic responses and to distinguish clearly between the soil flow and inertia effects. Monopiles in liquefiable soils are

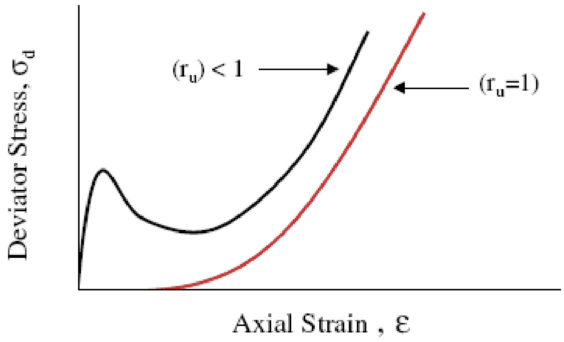

Fig. 1 The behavior of saturated sandy soil during the process liquefaction (Ashour and Ardalan 2011)

designed in a way to void failure regarding lateral loads arising from inertia and/or lateral spreading. The effect of some basic factors, such as the frequency of load, relative density, and peak acceleration, on the essential design features of monopiles such as displacement accumulation and bending moment are investigated.

2. Monopile-soil interaction mechanisms in liquefied soil

When a pile foundation embedded in a cohesionless soil is subjected to earthquake excitation, various mechanisms and processes are observed, including the following:

- *Stiffness degradation*: The high pore-water pressure (PWP) may yield a substantial degradation in the soil strength and stiffness. From the liquefied state, the soil stiffness is degraded due to the built-up excess PWP and thereafter increases, resulting in the post-liquefaction state. The stress–strain response of the soil due to the lateral push from the pile as the result of superstructure load can be as shown in Fig. 1. Similarity between the stress-strain and p-y curves was observed during the post-liquefaction period when $r_u = 1$ (Rollins *et al*. 2005). “S-shape” curves were reported from triaxial and centrifuge tests by Yasuda *et al*. (1999) and Wilson *et al*. (2000).
  Many authors have investigated the reduction in strength due to PWP generation, and numerous stiffness degradation models have been reported, such as the P-multiplier, C_u-factor, residual strength, and zero strength models for the liquefied soils (Liu and Dobry 1995, Brandenberg 2005, Goh and O’Rourke 1999, Bhattacharya *et al*. 2005).
- *Lateral spreading*: In most major earthquakes (e.g., San Francisco 1906, Alaska 1964, Niigata 1964, Loma Prieta 1989, and Kobe 1995), failure of the pile foundations in liquefiable soils during the earthquakes has been attributed to the effects of liquefaction-induced lateral spreading. Large ground displacements during these events caused substantial damage to harbor facilities, bridge and structure foundations, buried pipelines, and many infrastructure facilities (Hamada 1992, Tokimatsu 1999, Dobry and Abdoun 2001). Lateral spreading was initially reported by the National Research Council (1985) and has been characterized by centrifuge, shaking table, and laminar shear box tests. However, the Japanese Code of Practice (JRA 1996) is the only code to incorporate this terminology. The JRA assumes that, in the seismic pile-soil interaction, the soil pushes the

pile, leading to the bending mechanism. More recently, a simplified pseudo-static method was developed by Ishihara and Cubrinovski (2004) to present the *p-y* curves for piles in liquefied soil and to obtain the resultant soil pressure induced by lateral spreading. A reduction factor for the initial modulus (initial stiffness of *p-y* curve) of the subgrade reaction was proposed to represent the degradation of stiffness due to liquefaction and nonlinear behavior (Hamada 1992).

- <u>*Gapping effect*</u>: This effect refers to the formation of an opening between the pile shaft and the surrounding soil due to dynamic lateral loading. Observations from the 1989 Loma Prieta earthquake (Pender and Pranjoto 1996) provide examples of the gapping effect at the foundation of a railway bridge over a modest stream near Watsonville, California.
- <u>*Buckling and bending instabilities*</u>: In 2003, Bhattacharya investigated case histories regarding the buckling of 14 piles when the soil was fully liquefied. Using Euler criteria, he found that both lateral loads due to the inertia of the superstructure and kinematic loads from the lateral soil spreading may induce bending failure in the piles. In most of the classified pile damages, when the axial load in the pile was 50% or more of the buckling load, the foundation experienced substantial damage.

3. Classical model for a laterally loaded pile in liquefied soil

Monopile foundations were initially used by the offshore oil and gas industry and installed in the Gulf of Mexico by the American Petroleum Industry (API) in the 1950s and 60s, spreading to the North Sea in the 1970s. The *p-y* (lateral load-lateral displacement) curve in a BNWF model for normal soil conditions developed by API and different formulations have been presented by (Reese *el al.* 1974, Bogard and Matlock 1980, Scott 1980, Parker and Reese 1970, O'Neill and Murchison 1983, Dash *et al.* 2008).

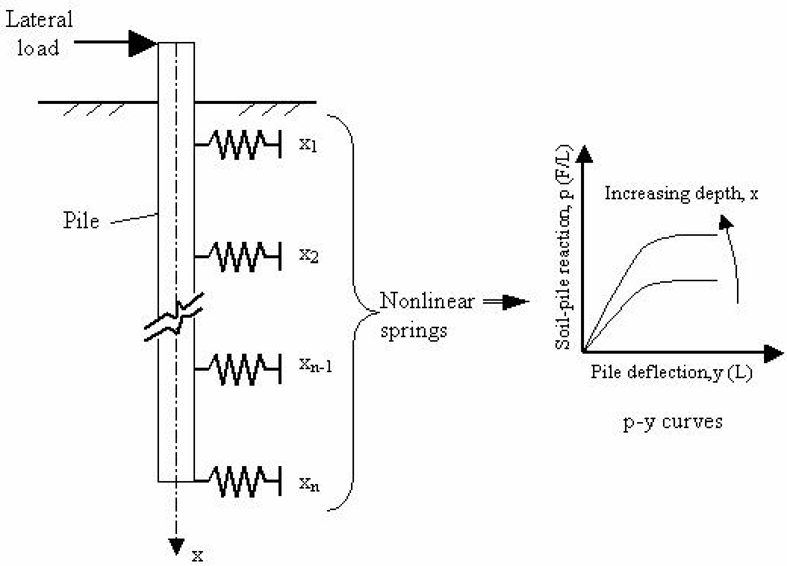

Fig. 2 Illustration of *p-y* method: *p* is the soil resistance and *y* is the horizontal displacement (API 2000)

The assessment of the dynamic response of offshore wind turbines differs from that of offshore oil and gas platforms and also onshore wind turbines. Offshore platforms are designed using static or quasi-static loads, whereas, offshore wind turbines need to have a non-linear dynamic analyses for an accurate assessment of both fatigue and ultimate limits states. Beside the number of load cycles, the natural frequency is another important parameter which should be somewhere between the wave and rotor frequencies (1P) or between 1P and 3P (for three bladed wind turbines). Because of these demands, the rotation and displacement of offshore monopiles under cyclic loading have shown to be the primary drivers in the design of offshore wind turbines (Kuo *et al*. 2012). The lack of available guidelines for offshore wind turbine structures drives the designers of offshore monopile foundations to employ the established design practice such as API by considering some correction factors (Sanjeev 2011). However, the validity of *p*-*y* curves for dynamic loading cases are controversial.

In contrast with adverse environmental loads for offshore monopile foundations, *p*-*y* method was developed for monotonic loading of small diameter piles based on the ultimate resistance and elastoplastic behavior of soil modeled by nonlinear distributed-uncoupled springs while the pile length is semi-infinite and soil's stiffness is constant, as shown in Fig. 2.

4. Model descriptions

A two-dimensional plane-strain analysis was performed with finite difference code (Itasca Consulting Group 2006) to solve the equation of motion by using lumped grid-point masses provided by the density of the surrounding zone. Converting 3-D problems of regularly spaced piles into 2-D plane strain models involves averaging the effect of actual 3-D structures over the spacing in the out-of plane direction (Lin and Feng 2006). The element spacing in out-of-plane direction is used to scale properties to approximate the 3-D effect which is associated with beam elements. "The spacing parameter is used to automatically scale properties and parameters to account for the effect of the distribution of the beams over a regularly spaced pattern" (Itasca Consulting Group 2006). Byrne constitutive relationships (Byrne 1991) have become available for loose sands to describe the generation of pore pressure adjacent to the pile shaft due to cyclic shear loading. The total soil medium was discretized into 1350 numbers of four-noded quadrilateral grids of 30 rows and 45 columns. The lateral dimension of each grid side was approximately 1.3 m. Fig. 3 depicts the finite difference discretization employed for simulations. Analyses were conducted on a pile with a circular cross-sectional diameter d of 6 m under 2 MN vertical loading which models the typical combined loading for an offshore wind turbine. In the numerical calculations, the pipe section of the monopile is replaced by a solid section pile with equivalent bending stiffness as proposed by Achmus *et al*. (2009).

The proposed analysis of the model boundaries encompassed two steps. First, the static

Table 1 Pile properties

Mechanical property of pile		Geometry of pile			
Density (kg/m^3)	Young's modulus (kPa)	Cross section area (m^2)	Cross section moment of inertia (m^4)	Total length (m)	Perimeter (m)
7800	2×10^8	1.853	8.06	30	18.84

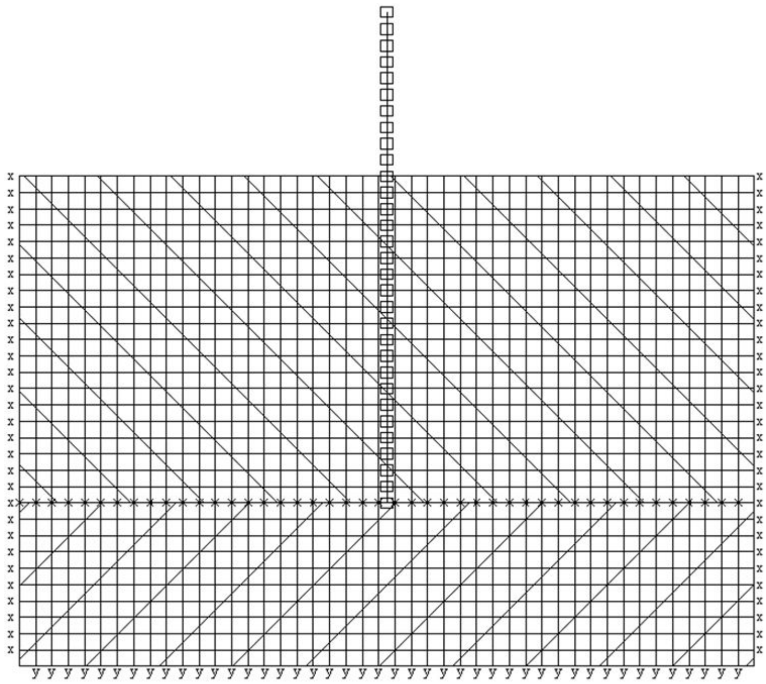

Fig. 3 Numerical model used to simulate the full-scale monopile

boundaries were defined by constraining the vertical boundaries from horizontal translation, while the base boundary was fixed against both horizontal and vertical translations. Second, the horizontal acceleration history was applied at the base, followed by the free-field boundary conditions at the two vertical sides to absorb the propagating wave from the system. To obtain the velocity time history in the case of transient loading, the filtered acceleration was integrated from the baseline-corrected acceleration time history.

The next section describes the steps involved in the numerical simulation of the static stability of the pile system and the dynamic loading.

4.1 Material properties

The soil was modeled with an elastoplastic Mohr-Coulomb constitutive model, characterized by a viscous soil damping ratio ξ of 5%. The pile was modeled with linearly elastic elements. The vertical steel piles were passed through a 20-m layer of loose medium sand (D_r = 40%) on a 10-m underlying layer of dense fine sand (D_r = 80%) (Fig. 4). The external radius and thickness of the monopile were 3 m and 0.1 m, respectively. The sand permeability used in the numerical analyses was scaled in terms of the unit weight of water.

4.2 Static equilibrium

Before the dynamic analysis begins, the model was set to a static equilibrium. The dynamic mode and water flow were set off. Based on the recommendation, the number of steps needed to remove all unbalanced forces should be more than 999 (Itasca Consulting Group 2006). The

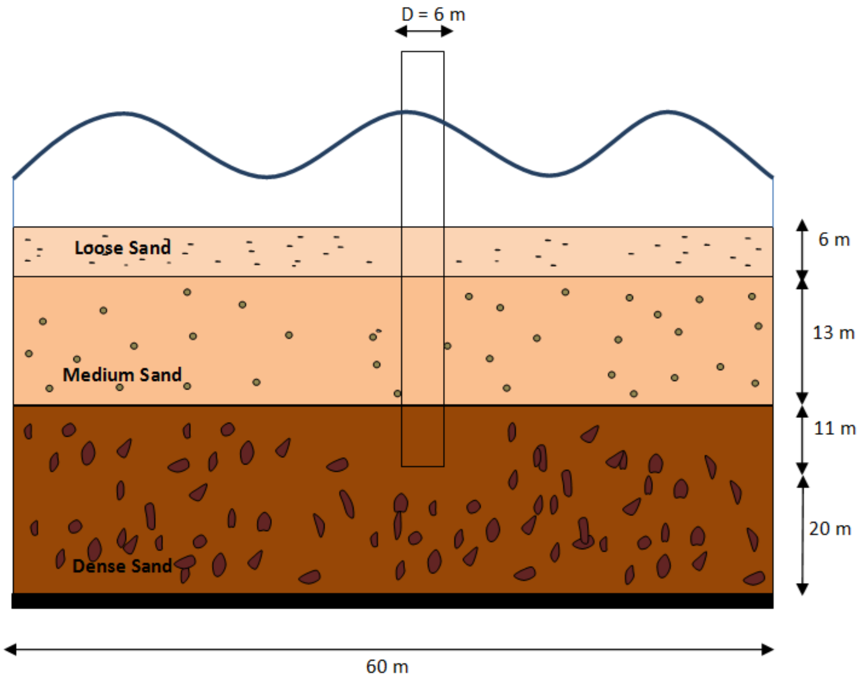

Fig. 4 Configuration of offshore monopile foundation model in this study

groundwater configuration generates pore pressure; however, there is no water flow. The initial stresses and pore pressure were set to those of the medium. The initial stresses and pore pressure values varied linearly through the depth of the medium. By considering water depth equal to 5 m the initial stress of 50 kPa at the ground level was assigned to the numerical model.

4.3 Dynamic pore-pressure generation model

The effective-stress analyses were carried out using modified Mohr-Coulomb failure criterion, and the strain softening model, which is appropriate for materials that show a degradation in shear strength when loaded beyond the initial failure limit. The effective-stress analyses is also engaged by Finn model that incorporates two equations correlating the volumetric strain induced by cyclic shear strain and excess pore water pressure produced during cyclic loading. The dynamic pore water pressure generation may be computed from formulations presented by Martin *et al*. (1975) and Byrne (1991) in which the volumetric strain developed during cyclic loading is dependent on the shear strain as well as previously accumulated volumetric strain.

The relation between the pore-pressure increment and irrecoverable volume-strain increment under the undrained condition can be expressed as

$$\Delta u = \overline{E_r}\Delta\varepsilon_{vd} \tag{1}$$

where Δu is the pore-pressure increment, $\overline{E_r}$ is the rebound modulus of the soil, and $\Delta\varepsilon_{wd}$ is the irrecoverable volume-strain increment. In dynamic formulations, based on the soil and fluid (water) displacement and the pore water pressure, the stiffness reduction occurs due to positive pore pressure development during liquefaction (Zienkiewicz *et al.* 1999). Noting that the relationship between the irrecoverable volume-strain and the cyclic shear-strain amplitude was independent of the confining stress, Martin *et al.* (1975) supplied the following empirical equation that relates the increment of the volume strain ($\Delta\varepsilon_{vd}$) to the cyclic shear-strain amplitude (γ)

$$\Delta\varepsilon_{vd} = C_1(\gamma - C_2\varepsilon_{vd}) + \frac{C_3\varepsilon_{vd}}{\gamma + C_4\varepsilon_{vd}} \tag{2}$$

where C_1, C_2, C_3 and C_4 are constants depending on the volumetric strain behavior of the sand. In Eq. (2), the volume-strain increment decreases as volume strain is accumulated. Byrne (1991) suggested the following modified and explicit model with two calibration parameters

$$\frac{\Delta\varepsilon_{vd}}{\gamma} = C_1 \exp\left[-C_2\frac{\varepsilon_{vd}}{\gamma}\right] \tag{3}$$

where C_1 and C_2 are constants with different interpretations from Eq. (2). C_1 can be derived from the relative density (D_r) as follows

$$C_1 = 7600(D_r)^{-2.5} \tag{4}$$

By using an empirical relationship between D_r and the normalized standard penetration test values, $(N_1)_{60}$

$$D_r = 15(N_1)_{60}^{0.5} \tag{5}$$

Therefore, $C_1 = 8.7(N_1)_{60}{}^{-1.25}$ and, in many cases, $C_2 = \dfrac{0.4}{C_1}$.

4.4 Soil-pile interaction model

In the present study, the piles were modeled as beam elements. Appropriate soil-pile interface properties (i.e., axial stiffness, normal stiffness, and shear stiffness) were scaled to represent the plane strain. The shear and normal stiffness were obtained as follows (Itasca Consulting Group 2006)

$$k_n \quad \text{or} \quad k_s = 10 \times \left[\frac{K + \frac{4}{3}G}{\Delta Z_{\min}}\right] \tag{6}$$

where K and G are the bulk and shear moduli of the soil zone, respectively, and $\Delta Z_{\min}$ is the smallest dimension of an adjoining zone in the normal direction. The cohesive strength of the shear coupling spring (in force per distance) is defined as the pile perimeter times the undrained cohesion of the soil (i.e., zero for the present study). The cohesive strength of the normal coupling spring (i.e., zero for the present study) can be modeled as the limiting lateral resistance and computed based on Broms solution (Broms 1964) as $9 \times S_u \times D_p$, where D_p is the pile diameter.

In order to model end bearing capacity, authors adjusted the related properties of the corresponding shear spring by assigning the proper values via the coupling spring shear stiffness and the cohesive strength values and by neglecting shear friction along the bottom segment of the pile.

5. Numerical results

5.1 Verification of the solution

For the verification of the results, the centrifuge test data reported by Wilson *et al*. (2000) for single steel piles with a length of 18.8 m, outer diameter of 0.67 m, and wall thickness of 0.019 m were considered.

The above mentioned centrifuge tests were modeled numerically using the finite difference code FLAC. Wilson *et al*. (2000) presented four different layouts, with each model characterized by two horizontal layers of saturated uniformly graded Nevada sand (Table 2). The relative density (D_r) of the lower layer was about 80% for all layouts. The pile experienced a superstructure load of 480 kN at 3.8 m above the ground surface. The properties of Nevada sand have been reported by Popescu and Prevost (1993) and are tabulated in Table 3. In 2005, Liyanapathirana and Poulos developed a one-dimensional, finite element-based numerical model for analyzing piles founded in liquefying soil. An effective stress-based free-field ground response analysis was initially used to determine the movement of the external soil, the degradation of the soil stiffness, and the strength due to the generation of pore pressure.

Wilson *et al*. (2000) and Liyanapathirana and Poulos (2005) demonstrated the ability of the numerical FDM by comparing the results from simulated monopile model in liquefying soil with those from centrifuge tests. The FDM model was shaken with acceleration records scaled to 0.22 g and 0.45 g, similar to those of the Kobe 1995 and Santa Cruz 1989 earthquakes. The soil medium in the numerical model was divided into two soil layers with the same depth and properties as

Table 2 Earthquake events

Container	Event	Motion	$a_{\max,base}$ (g)	Density of upper sand layer
Csp2	D	Kobe	0.04	35%
Csp2	J	Santa Cruz	0.45	35%
Csp3	J	Kobe	0.22	55%
Csp3	M	Santa Cruz	0.41	55%

Table 3 Soil properties for the parametric analysis (Popescu and Prevost 1993)

Properties	D_r = 40%	D_r = 55%	D_r = 80%
Density (kg/m^3)	2670	2670	2670
Bulk modulus, K (Pa)	216×10^6	292×10^6	432×10^6
Shear modulus, G (Pa)	27×10^6	30.2×10^6	44.7×10^6
Friction angle, ϕ	33°	34.2°	39.5°
Porosity	0.424	0.406	0.373
Permeability, k (m/s)	6.6×10^{-5}	6.05×10^{-5}	3.7×10^{-5}
$(N_1)_{60}$	7.2	14	30

adopted in the centrifuge test. The total soil medium was discretized into 880 finite difference grids in 44 rows and 20 columns, and the pile was divided into 19 equal segments. Good correspondence was obtained between the measured and computed pore pressures at depths of 3.8 and 4.6 m, as shown in Figs. 5 and 6. The coincidence of sharp pore pressure decreases and acceleration spikes may be attributed to transition from contractive to dilatants behavior resulting from de-liquefaction shock waves (Kutter and Wilson 1999). The numerical simulation has been shown to predict the steady state response of pore pressure development realistically. However, the model may not be used to distinguish the pile response as a function of dilation angle.

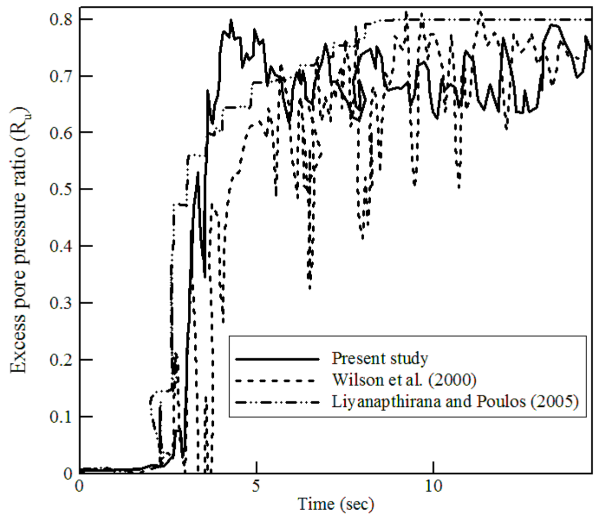

Fig. 5 Comparison of time histories of pore pressure ratio at the 4.6 m depth from surface for Kobe earthquake, $a_{\max,base}$ (g) = 0.22 g

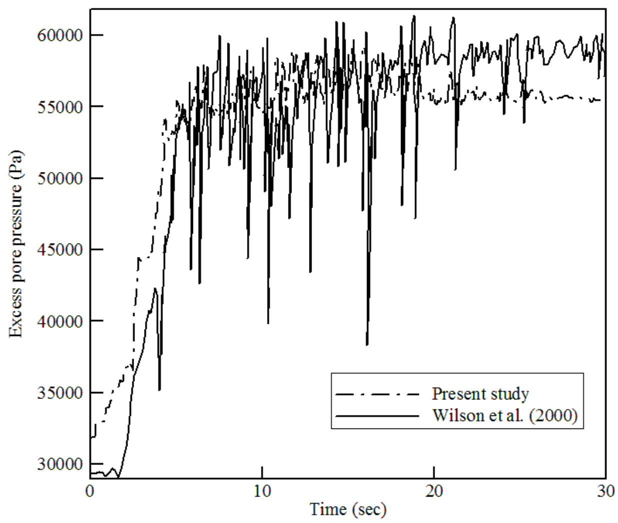

Fig. 6 Comparison of time histories of excess pore pressure at the 3.8 m depth from surface for Santa Cruz earthquake, $a_{\max,base}$ (g) = 0.45 g

From figure in this section it can be mentioned that the steady state behaviour of excess pore pressure was modeled properly which makes the soil liquefied. The coincidence of reductions in excess PWP and load spikes might be related to the dilation behavior in soil adjacent the pile shaft and this observation would be addressed in subsequent works of authors.

5.2 Case study of monopile

In the present study, five ground-motion records with different predominant frequencies (i.e., Kobe, Loma Prieta, Santa Cruz, Morgan Hill, and Kocaeli earthquakes) were considered for the dynamic analysis of an offshore monopile. For each earthquake, the acceleration time was defined at the outcropping bedrock considered to be representative of four duration scenarios. Data were taken from the Pacific Earthquake Engineering Research Center (PEER) database and scaled to 0.1 g, 0.2 g, and 0.3 g peak acceleration values. The cubic baseline-corrected scaled earthquake data were used for all combinations of soil and pile parameters. Table 4 summarizes the details of the earthquake records.

To illustrate some important features of ground displacements in liquefied soils, observations from the numerical modeling of an offshore monopile model subjected to 2 MN superstructure load and the motion from the well-documented Loma Prieta earthquake are discussed herein. Two different models without and with superstructure load are considered. In order to take advantage of tower inertia effect along with the kinematic flow of soil, massive monopile foundation with certain distance from ground level is modeled in section 5.3 (see Achmus *et al*. 2013, Zafeirakos and Gerolymos 2013). The acceleration time histories at the soil base are shown in Fig. 7.

5.2.1 Results and discussion for the monopile, considering the kinematic loads

This section presents the results of a monopile subjected to strong Loma Prieta ($a_{\max,base}$ = 0.3 g) motion (PEER 2013). An axial load of 2000 kN load is considered at the monopile head.

5.2.1.1 Cyclic ground displacements

To identify the pattern of ground displacement for the free fields, which are areas that are particularly vulnerable to lateral spreading during seismic loading, the excess PWP and horizontal ground displacement values during the Loma Prieta earthquake (1989) were computed, as shown in Fig. 8.

Based on the fully coupled porous media-pore fluid dynamic FDM, the shaking time in which the sand was initially in the state of limited liquefaction was 6.5 s. Cyclic horizontal ground

Table 4 Earthquake data

Earthquake name	Santa Cruz	Morgan Hill	Loma Prieta	Kobe	Kocaeli
Date of earthquake	17/10/89	24/04/84	18/10/89	16/01/95	17/08/99
Station of earthquake	-	57191 Halls Valley	47380 Gilroy Array	-	Sakarya
PGA of earthquake (m/s^2)	0.1 g, 0.2 g, and 0.3 g	0.1 g, 0.2 g, and 0.3 g	0.1 g, 0.2 g, and 0.3 g	0.1 g, 0.2 g, and 0.3 g	0.1 g, 0.2 g, and 0.3 g
Duration of earthquake (s)	30	40	30	15	50
Predominant frequency (Hz)	1.67	1.79	2.63	2.78	6.42

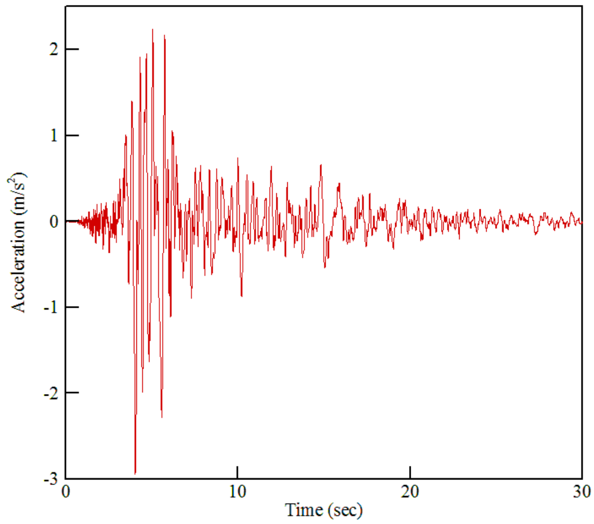

Fig. 7 Loma Prieta (1989) acceleration time history at the base level (PEER 2013)

displacements in the instant of ground shaking had peak values of about 5 cm. These observations are consistent with the peak value of shear strain (about 6.2%) throughout the 8-11 m of liquefied layer depth that was prone to instability. Surprisingly, at the instant that the ground experienced a lateral deformation of about 5 cm from the start of shaking, the excess PWP was distinctly below the effective overburden pressure (Fig. 8(a)). This finding may indicate that the soil had not yet fully liquefied at this stage. These peak lateral ground deformations are consistent with the high ground acceleration of about 3.2 s at the ground surface.

The actual lateral monopile-soil interaction during the flow of liquefied soil appears to be complex, because the peak ground displacements and accelerations coincided just before the development of full liquefaction. The hypothesis of monopile behavior in liquefied soil is assumed, to consider the combination of lateral loads due to the inertia of the superstructure and/or kinematic loads due to ground displacements during the cyclic phase, which may induce bending moments in the monopile. The associated lateral loads due to these events depend on the predominant periods of the pile and the relative displacement between the soil and pile.

5.2.1.2 Pore fluid migration

Before the discussion is continued, it is important to define components of this performance-based design. The excess PWP ratio (R_u) is defined as the ratio of the difference between the initial and current mean effective stresses over the initial effective stress (Cheng and Jeremic 2009)

$$R_u = \frac{P_{initial} - P_{current}}{P'_{initial}} \tag{7}$$

Of particular interest are the steady-state and the maximum values of R_u. The steady-state value is a constant value of R_u that is reached for a certain period of time at the end of shaking. As shown in Fig. 9, the excess PWP values increased dramatically during the first 5 s of shaking for nearly all depths and remained relatively constant after about 10 s up to 30 s. Given the characteristics of liquefaction (i.e., R_u), the kinematic mechanism, and the lack of inertial effects throughout the top 12-m layer, the calculation of excess PWP values was restricted to a 12-m soil layer. In this analysis, the seismic shaking developed the free-field excess PWP, thereby reducing the strength of the saturated loose sand adjacent to the monopile.

The zone of liquefaction (h_L) for a given depth was calculated as the R_u value become greater or equal to 1 after an associated drop in the confining effective pressure. Fig. 10 shows the zone of liquefaction at different times. The R_u value was greater than or equal to 1 for a depth of 11 m at 10 s excitation. Hence, this region was classified as a fully liquefied zone.

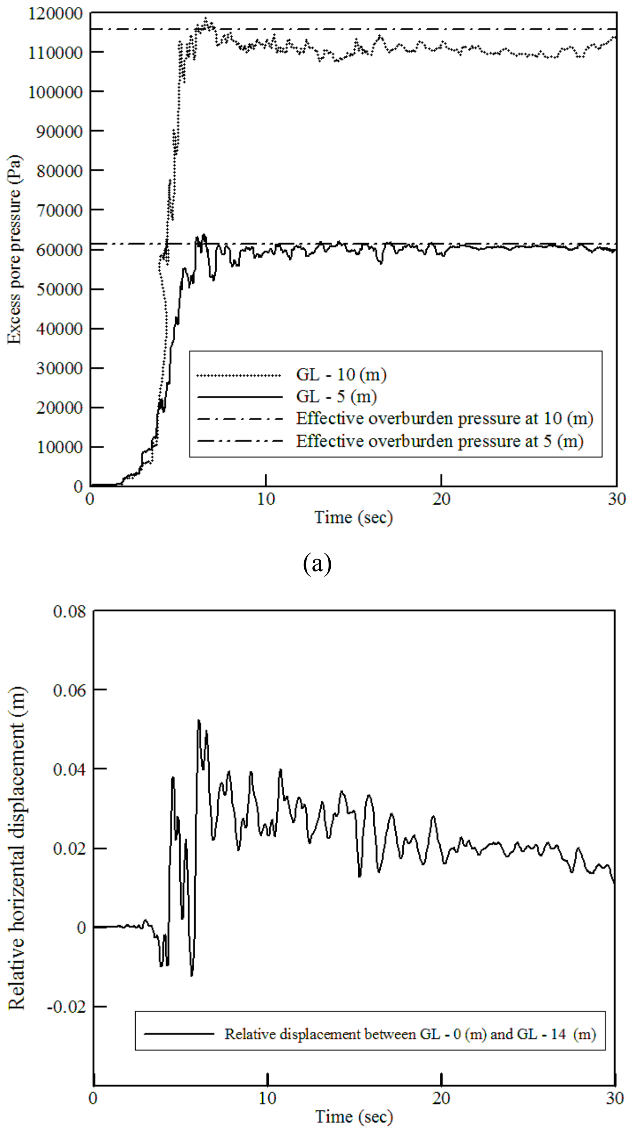

Fig. 8 Excess pore water pressures and ground displacements in a liquefied deposit

5.2.1.3 Shear strain

When loose sand is subjected to ground motion, a high shear strain develops, leading to soil liquefaction (Kramer 2003). In most cases, it is very difficult to obtain a reliable prediction for the shear strain of the liquefied soil. Fig. 11 presents the shear strains throughout the depth of the liquefied layer, are presented based on the continuum model for porous media. The shear strain increased up to 4.8% at a depth equal to 5 m from the ground surface.

5.2.1.4 Monopile behavior in areas of seismic liquefaction

Fig. 12 shows the development of the bending moment along the monopile length during

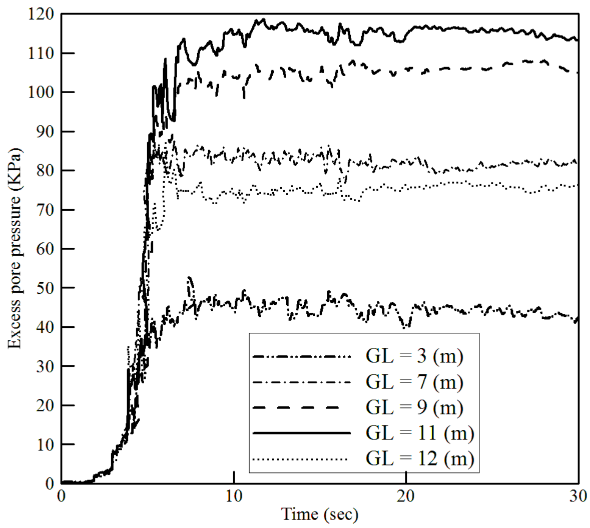

Fig. 9 Excess pore water pressure at different depths

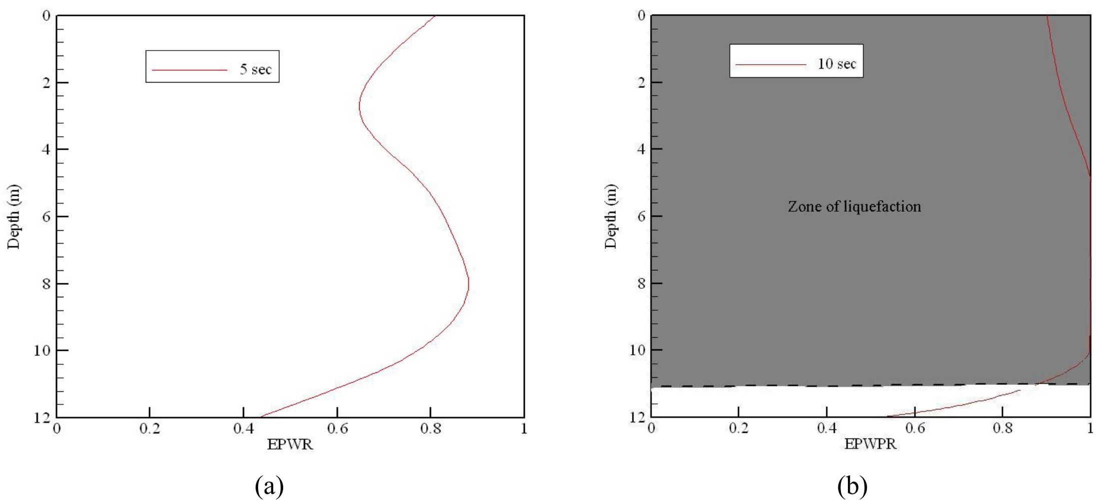

Fig. 10 Zone of liquefaction at different time instant

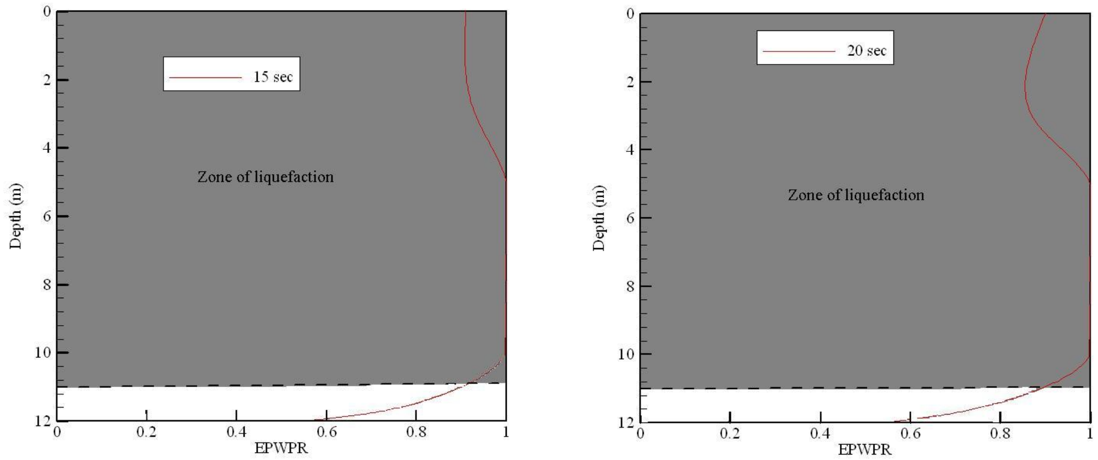

(c) (d)

Fig. 10 Continued

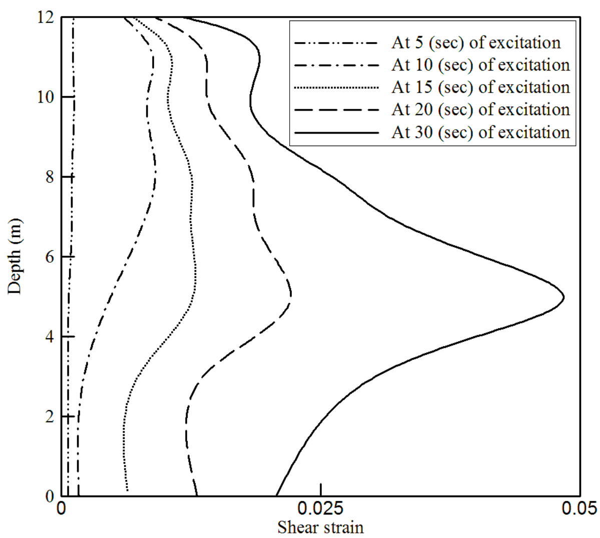

Fig. 11 Shear strain in the liquefied zone

shaking. The maximum bending moment profile is shown for a D_r of 40%, a_{max} of 0.3 g, and monopile diameter of 6 m (Fig. 12). Under this loading condition, the maximum bending moment (M_{max} = 1985 kNm) occurred at a lower portion of the pile close to the liquefied and non-liquefied border, a phenomenon referred to as the "bottom-up effect" (Ishihara 1997), during the early stages before soil liquefaction (t = 5 s).

Given the severe damage that was inflicted to pile structures during the 1995 Kobe earthquake, recent research on failure mechanisms involved in the soil-pile interaction has drawn considerable attention. Japanese design specifications for highway bridges were revised after this earthquake, with new guidelines accounting for the forces due to liquefaction-induced ground movement. In this section, the inertial effects on the monopile are ignored. Therefore, the flow of top 20-m of liquefied soil is considered to be the only external source of lateral force on the pile. A schematic view of the model based on the JRA (1996) code for fully water-submerged piles is shown in Fig. 13.

Based on the JRA (1996) code, 30% of the total overburden pressure due to water is considered to be the maximum soil flow pressure at ground level (point A)

$$F_A = 30\% \text{ of total overburden pressure} = 0.3 \times 5 \times 10\,(\text{kN/m}^3) = 15\,\text{kPa} \tag{8}$$

By using the same strategy, the maximum lateral kinematic pressure at a depth of 11 m acting at point B is

$$F_B = 30\% \text{ of total overburden pressure} = 0.3 \times \left(5 \times 10\,(\text{kN/m}^3) + 11 \times 27.6\,(\text{kN/m}^3)\right) = 106\,\text{kPa} \tag{9}$$

where the soil density is 27.6 kN/m^3. Finally, the maximum moment should occur at point B in Fig. 13, due to the spreading force from the trapezoidal zone

$$M_{\max(JRA)} = 15 \times 11 \times 11/2 + 91 \times 11 \times 11/6 = 2742.77\,\text{kNm} \tag{10}$$

This calculation shows that the induced moment by flowing soil is over-predicted by the JRA approach as compared to the FDM analysis

$$M_{\max(JRA)} > M_{\max(FDM)} \tag{11}$$

Keep in mind that the tower interaction and lateral loads due to wind and wave have not been considered in the presented simulation. The maximum bending moment increases by considering additional load conditions.

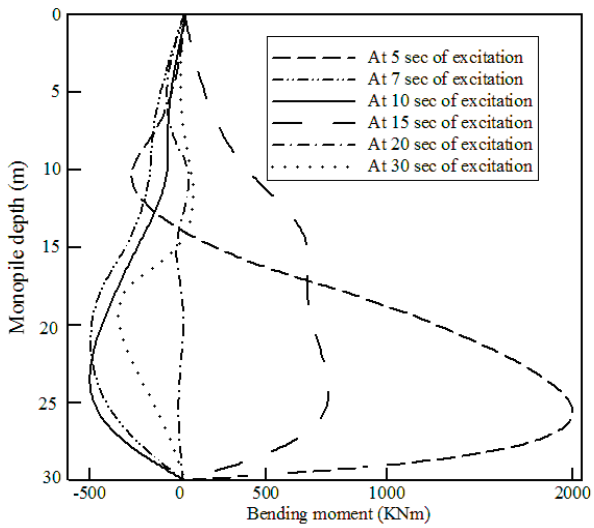

Fig. 12 Bending moment profile versus monopole depth

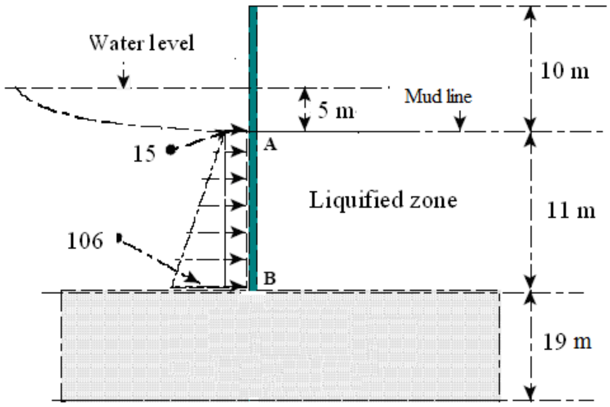

Fig. 13 Schematic diagram showing the predicted load based on the JRA code (JRA 1996)

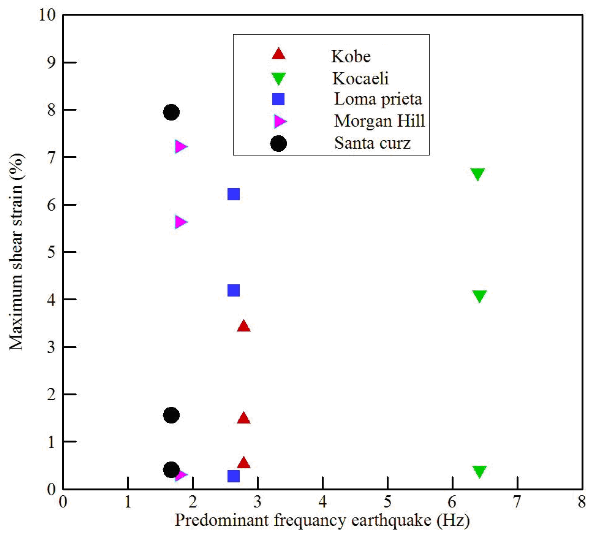

Fig. 14 The maximum shear strain for different predominant frequencies of earthquake at different maximum accelerations

5.2.2 Effect of the earthquake parameters

Time history data from five earthquakes with different predominant frequencies were considered for this analysis (see Table 4 for details). The acceleration time data for each earthquake were scaled to 0.1 g, 0.2 g, and 0.3 g. The maximum bending moment and shear-strain values at different depths were obtained. Fig. 14 shows the maximum shear-strain values for different peak acceleration values (a_{max}) with respect to the earthquake predominant frequencies. The maximum shear-strain values were significantly influenced by the a_{max} values, with the maximum shear-strain in the soil increasing with increasing a_{max}. According to the numerical analyses, a maximum shear-strain of about 8% occurred during the Santa Cruz Earthquake with an a_{max} of 0.3 g. Lower maximum shear-strain values of 0.5% and 1.6% were obtained for the models with a_{max} values of 0.1 g and 0.2 g, respectively. Thus, the maximum shear-strain value decreased

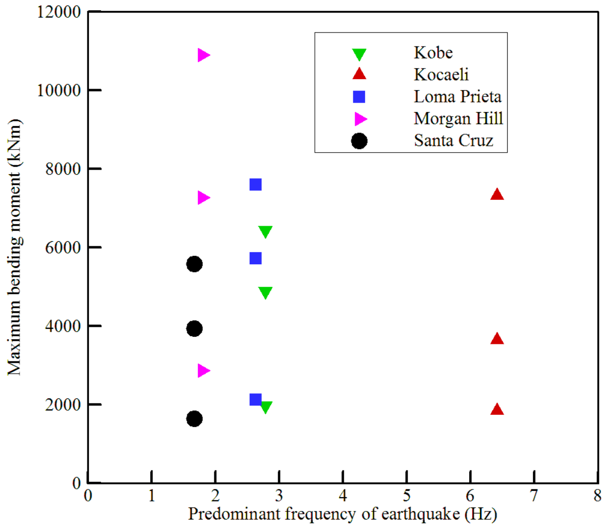

Fig. 15 The maximum bending moment for different predominant frequencies of earthquake at different maximum accelerations

when the predominant earthquake frequency value increased for a given value of a_{max}. The discrepancies in Fig. 14 can be ascribed to the dependency of the resultant shear strains on the maximum acceleration of motion, the predominant frequency of motion, and the fundamental frequency of the liquefied soil.

Fig. 15 compares the maximum bending moments observed in the numerical analyses for different earthquake parameters. The location of a plastic hinge due to flowing soil and lateral spreading is expected to occur at the interface of the liquefiable and non-liquefiable layers, because this section experienced the highest bending moment. The maximum bending moment decreased with the decrease in maximum acceleration: for example, for a_{max} values of 0.1 g, 0.2 g, and 0.3 g, the M_{max} values were 10900, 7280, and 2860 kNm, respectively, with a predominant frequency of 1.79 Hz; and the M_{max} values were 7320, 3636, and 1836 kNm, respectively, with a predominant frequency of 6.42 Hz. Thus, the M_{max} values decreased with the increase in the predominant frequencies.

5.2.3 Response of the monopile considering the inertia-kinematic effects

This section presents the results of a monopile subjected to 0.3g acceleration (Loma Prieta earthquake). A superstructure mass of 2000 kN load is considered at the monopile head.

5.2.3.1 Pore fluid distribution

Fig. 16 shows the excess PWP responses at 12 different points along the depth. Two different cases are defined. Case I contains 6 points for modeling the behavior of pore fluid in soil adjacent to the monopile shaft. Case II models the free-field behavior, with points chosen approximately midway (point from free-field) between the pile and the vertical boundary.

Moving into the deeper soil layers, the lower layers do not liquefy and the pore fluid rapidly dissipates upwards. As a result of the pumping effect, the upper soil layers initially reach only limited or fully liquefied states.

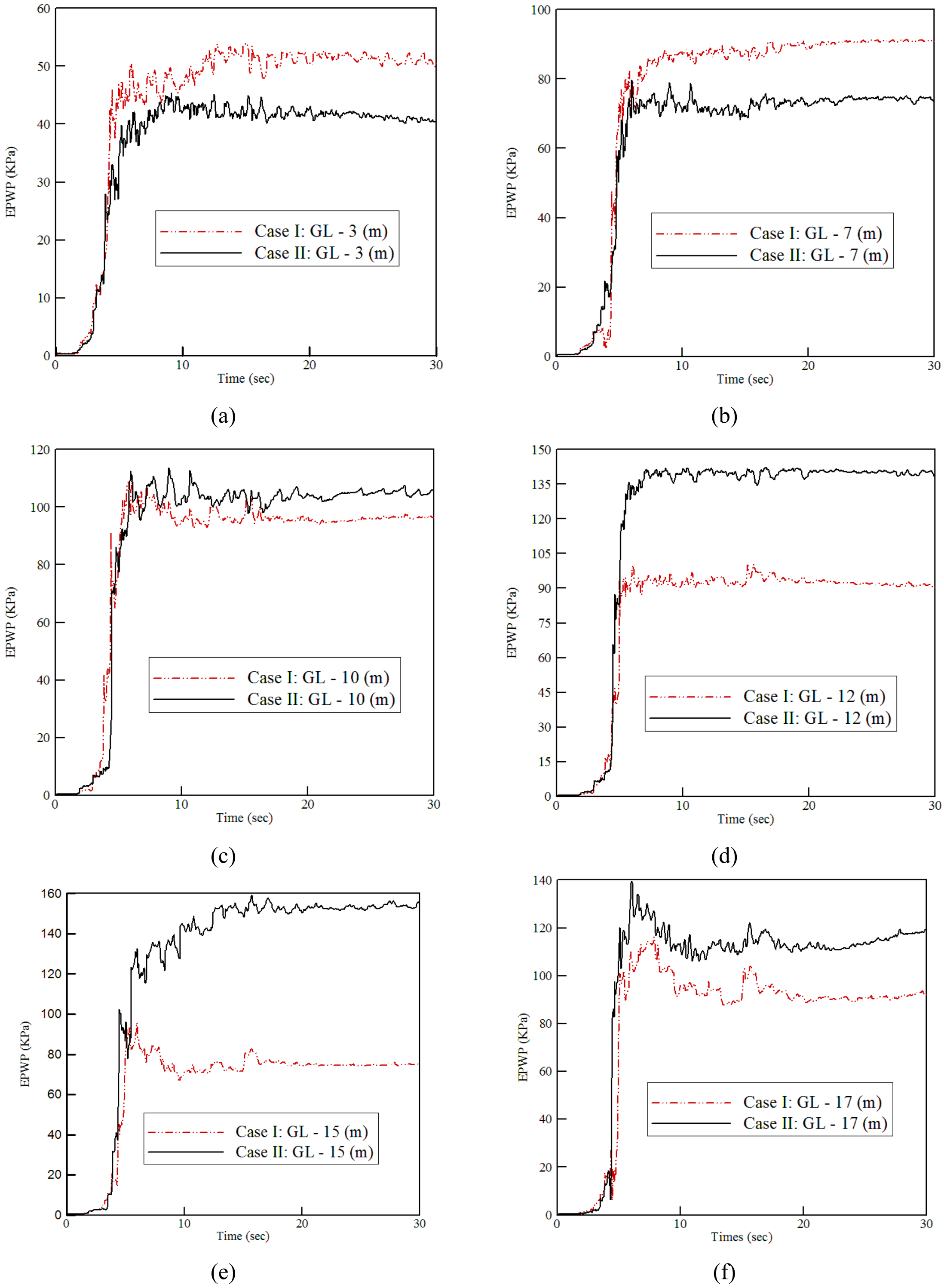

Fig. 16 Excess pore pressure time histories for different soil elements for cases I and II at different ground level

The system of a monopile with a mass on top displayed an increased R_u value during shaking for the top elements compared to the value in the free field. The pile-column-mass (PCM) system interrupted the dynamic characteristics of the top layers, where the monopile tended to create compressive and extensive deformations. Meanwhile, inertial effects from the superstructure during seismic excitation created an additional volume-shearing deformation field at the ground level in the soil adjacent to the monopile, leading to additional compression of the soil fabric and pore fluid volume. Of particular interest are the excess PWP results for the middle layers (10 m) where the differences between cases I and II were fairly small. However, below a distinct level at which the inertial effect was less significant, the simulated excess PWP in case II (free-field) was significantly larger than that for the same level in case I. This finding can be explained by the hypothesis that the monopile stabilizes the lower soil layers and prevents excess shear deformation in the adjacent soil above the monopile base.

5.2.3.2 Monopile response

The results from the previous sections clearly show that the pile response is markedly influenced by the characteristics of the earthquake. Other significant patterns are consistently found at various depths for many inspected monopiles, reflecting the complex dynamic nature of loads and the behavior of piles in liquefying soils. Next, bending envelopes are considered to analyze these patterns.

The behavior of the bending moment that is induced in the monopile-soil interaction in the presence of a superstructure mass depends on the kinematic forces from the flowing soil. As shown in Fig. 17, the bending moment is a function of the liquefied zone. The bending moment was attained at soil depths ranging from 5 to 15 m, with a peak moment of 3374 kNm at about 4 s. The maximum bending moment $M_{\max}$ to develop in the pile after liquefaction was 13240 kNm at 4.6 s, significantly larger than the moment of 7600 kNm when only lateral spreading was present. The bending moment observed in the monopile base was due to the restraint and differential pressure on the pile bottom from the soil. The negligible moments that developed throughout the

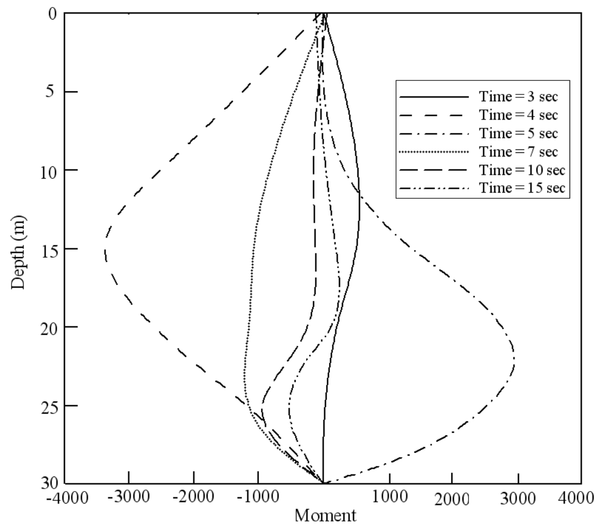

Fig. 17 Developing the bending moment versus depth in terms of shaking time in presence of mass inertia

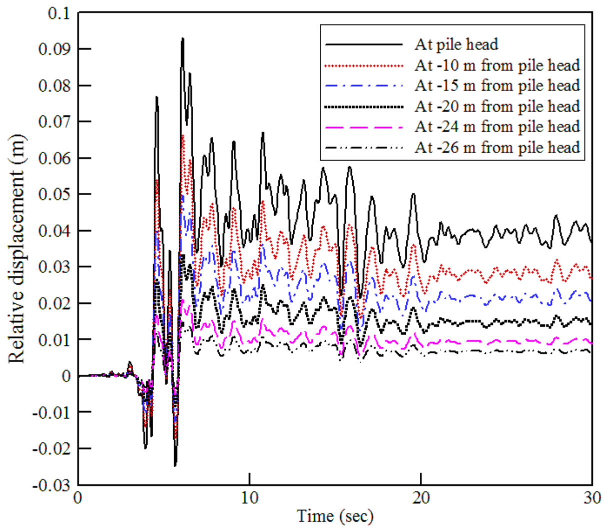

Fig. 18 Relative displacement of monopile at different levels with respect to the monopile base in presence of mass inertia for different levels

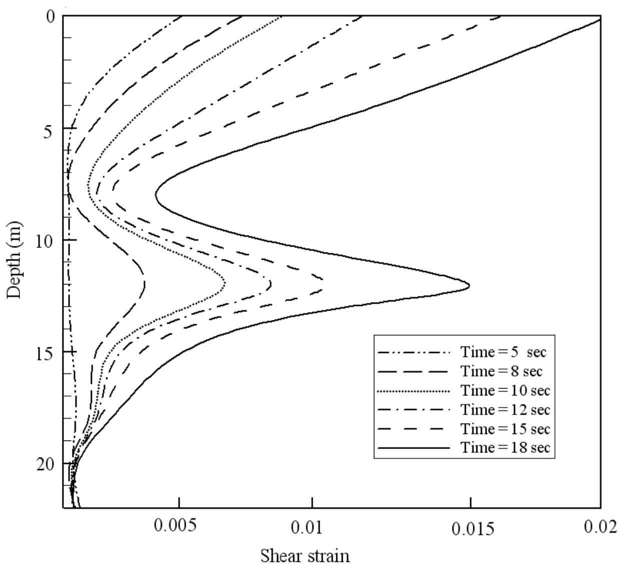

Fig. 19 Development of shear strain in the liquefied soil in presence of inertia effect

lower part of monopile show that the curvature of the monopole needs to be changed along the depth.

Lateral displacement of piled foundations during liquefaction can be severely damaging during earthquake shaking (Tokimatsu *et al*. 1996). The relative lateral displacements of the monopile head were evaluated before and after the complete liquefaction of soil. Fig. 18 outlines the relative displacements of the monopile in the presence of axial loads from the superstructure and lateral spreading. The lateral displacement of the pile gradually increased just after liquefaction, reaching a steady state. The analysis predicted a lateral deflection of the pile head of about 0.11 m before the onset of liquefaction.

5.2.3.3 Soil skeleton deformation

At the onset of shaking, the inertial forces of a 2-MN superstructure load were transferred to the top of the pile and ultimately to the soil. The top-down effect postulated by Ishihara (1997) is clearly shown in Fig. 19, because the upper layers underwent significant deformation (i.e., shear strain of 2% at GL-0 m). As significant shearing with PWP build-up developed in the lower soil layers, those layers contributed to most of the bottom-up effect (i.e., shear strain of 1.5% at GL-12 m). Interestingly, the effect of inertia was more pronounced than lateral spreading for the monopiles in liquefiable soils.

It is interesting to note that the shear strain is changed dramatically in the liquefied layer and the pile load-carrying capacity decreases regardless of designing approach based on failure mode (Haldar *et al*. 2008, Haldar and Babu 2010).

6. Conclusions

In reality, the behavior of the lateral monopile-soil interaction during earthquake-induced liquefaction is very complex, and no standard design procedure yet exists for laterally loaded monopiles in liquefiable soils.

Considering the above-mentioned issue, the following conclusions can be drawn from the current study.

(a) Herein, the effects of inertial and kinematic loads induced by ground motions with variable predominant frequencies were examined by using numerical calculations with a large-diameter monopile.

(b) Offshore monopiles are dynamically sensitive structures to the loading frequency, which is mainly due to the possible accumulation of pore water pressure with every cycle. The excess PWP build-up in an underlying sand deposit during an earthquake may yield a substantial degradation in soil strength and stiffness. The methodology given evaluates the near-field and free-field excess pore water pressure in the liquefied soil adjacent to the monopile shaft and the associated phenomena. The results thus present an intriguing challenge due to the slight increase of soil settlement at the monopile-head level. This can be described by the fact that the soil at shallow depths has the chance to drain partially excess pore water pressure towards the soil surface. Further research is required to understand more clearly the soil settlements induced by the long-term cyclic loading of offshore wind turbines.

(c) The application of a lateral inertial load made the monopile more laterally unstable. The bending moment in the monopile increased just after liquefaction, when an additional moment developed due to the lateral displacement of the monopile. The results showed that the maximum bending moment of the monopile was more pronounced through the ground deformation than the acceleration on the superstructure.

(d) The results reveal that the progressive reduction of soil stiffness due to liquefaction is a significant outcome in design procedure of wind turbine support structures. It was also found that an efficient and optimal design of the monopile-supported offshore wind turbine calls for considering tower inertia effect.

References

Achmus, M., Kuo, Y.S. and Abdel-Rahman, K. (2009), "Behavior of monopile foundations under cyclic lateral load", *Comput. Geotech.*, **36**(5), 725-735.
Achmus, M., Akdag, C.T. and Thieken, K. (2013), "Load-bearing behavior of suction bucket foundations in sand", *Appl. Ocean Res.*, **43**, 157-165.
AIJ, Architectural Institute of Japan (1988), *Recommendations for Design of Building Foundations*. [In Japanese]
American Petroleum Institute (2000), *Recommended Practice for Planning, Designing and Constructing Fixed Offshore Platforms – Working Stress Design*, API recommended practice 2A-WSD (RP2A-WSD), (21st Ed.), Dallas, TX, USA.
Ashour, M. and Ardalan, H. (2011), "Piles in fully liquefied soils with lateral spread", *Comput. Geotech.*, **38**(6), 821-833.
Barari, A. and Ibsen, L.B. (2012), "Undrained response of bucket foundations to moment loading", *Appl. Ocean Res.*, **36**, 12-21.
Bhattacharya, S. (2003), "Pile instability during earthquake liquefaction", Ph.D. Thesis, University of Cambridge, Cambridge,UK.
Bhatacharya, S. (2006), "Safety assessment of existing piled foundations in liquefiable soils against buckling instability", *ISET J. Earthq. Technol.*, **43**(4), 133-146.
Bhattacharya, S., Bolton, M.D. and Madabhushi, S.P.G. (2005), "A reconsideration of the safety of piled bridge foundations in liquefiable soils", *Soil. Found.*, **45**(4), 13-25.
Bogard, D. and Matlock, H. (1980), "Simplified calculation of *p-y* curves for laterally loaded piles in sands", Unpublished Report; Earth Technology Corp.
Brandenberg, S.J. (2005), "Behavior of pile foundations in liquefied and laterally spreading ground", Ph.D. Thesis, University of California, Davis, CA, USA.
Breton, S.P. and Moe, G. (2009), "Status, plans and technologies for offshore wind turbines in Europe and North America", *Renew. Energy*, **34**(3), 646-654.
Broms, B.B. (1964), "Lateral resistance of piles in cohesionless soils", *J. Soil Mech. Found Div. ASCE*, **90**(3), 123-156.
Butterfield, R. and Gottardi, G. (1996), "Simplified failure-load envelopes for shallow foundation on dense sand", *Int. J. Offshore Polar Eng.*, **6**(1), 62-67.
Byrne, P. (1991), "A cyclic shear-volume coupling and pore-pressure model for sand", *Proceedings of the 2nd International Conference on Recent Advances in Geotechnical Earthquake Engineering and Soil Dynamics*, St. Louis, MO, USA, March, pp. 47-55.
Cheng, Z. and Jeremic, B. (2009), "Numerical modeling and simulation of pile in liquefiable soil", *Soil Dyn. Earthq. Eng.*, **29**(11-12), 1405-1416.
Dash, S.R., Bhattacharya, S., Blakeborough, A. and Hyodo, M. (2008), "*P-Y* curve to model lateral response of pile foundations in liquefied soils", *Proceedings of the 14th World Conference on Earthquake Engineering*, Beijing, China, October.
Depina, I., Le, T.M.H., Eiksund, G. and Benz, T. (2013), "Cyclic behavior of laterally loaded piles in soils with variable properties", *Proceedings of the 23rd International Offshore and Polar Engineering Conference*, Anchorage, AK, USA, June-July.
Dobry, R. and Abdoun, T. (2001), "Recent studies on seismic centrifuge modelling of liquefaction and its effect on deep foundation", *Proceedings of the 4th International Conference on Recent Advances in Geotechnical Earthquake Engineering and Soil Dynamics* (Symposium in Honour of Professor W.D. Liam Finn), San Diego, CA, USA, March.
Goh, S. and O'Rourke, T.D. (1999), "Limit state model for soil-pile interaction during lateral spread", *Proceedings of the 7th US Japan Workshop on Earthquake Resistant Design of Lifetime Facilities and Countermeasures Against Soil Liquefaction*, Seattle, WA, USA, August, pp. 237-260.
Haldar, S. and Babu, G.L.S. (2010), "Failure mechanism of pile foundations in liquefiable soil: Parametric

study", *Int*. *J*. *Geomech*., **10**(2), 74-84.

Haldar, S., Babu, G.L.S. and Bhattacharya, S. (2008), "Buckling and bending response of slender piles in liquefiable soils during earthquakes", *Geomech*. *Geoeng*.: *Int*., **3**(2), 129-143.

Hamada, M. (1992), "Large ground deformations and their effects on lifelines: 1964 Niigata Earthquake, Case studies of liquefaction and lifelines performance during past earthquake", Technical Report NCEER-92-0001; Volume 1, Japanese case studies, National Centre for Earthquake Engineering Research, Buffalo, NY, USA.

Ibsen, L.B., Barari, A. and Larsen, K.A. (2012), "Modified vertical bearing capacity for crcular foundations in sand using reduced friction angle", *Ocean Eng*., **47**, 1-6.

Ibsen, L.B., Barari, A. and Larsen, K.A. (2014), "An adaptive plasticity model for Bucket foundations", *J*. *Eng*. *Mech*., **140**(2), 361-373.

Ishihara, K. (1993), "Liquefaction and flow failure during earthquakes", *Geotechnique*, **43**(3), 351-451.

Ishihara, K. (1997), "Geotechnical aspects earthquake", *Proceedings of the 14th International Conference on Soil Mechanics and Foundation Engineering* (*ICSMFE*), Hamburg, Germany, September, pp. 2047-2073.

Ishihara, K. and Cubrinovski, M. (2004), "Case studies of pile foundations undergoing lateral spreading in liquefied deposits", *Proceedings of the 5th International Conference on Case Histories in Geotechnical Engineering (*CD-ROM*)*, New York, NY, USA, April.

Itasca Consulting Group, Inc. (2006), "Fast Lagrangian Analysis of Continua (FLAC)", User's Manual, Version 5.0, Minneapolis, MN, USA.

Jiang, S.C., Wang, Z. and Zhao, X.L. (2011), "Structural performance of pre-stressed grouted pile-to-sleeve connections", *Procedia Eng*., **14**, 304-311.

JRA (1996), "*Specification for Highway Bridges*", Part V, Seismic Design. Japanese Road Association.

Kramer, S.L. (2003), *Geotechnical Earthquake Engineering*, Pearson Education, New Delhi, India.

Kuo, Y.S., Achmus, M. and Abdel-Rahman, K. (2012), "Minimum embedded length of cyclic horizontally loaded monopiles", *J*. *Geotech*. *Geoenviron*. *Eng*., **138**(3), 357-363.

Kutter, B.L. and Wilson, D.W. (1999), "De-liquefaction shock waves", *Proceedings of the 7th US-Japan Workshop on Earthquake Resistant Design of Lifeline Facilities and Countermeasures Against Soil Liquefaction*, Seattle, WA, USA, August, Volume 19, pp. 295-310.

Lesny, K. and Hinz, P. (2007), "Investigation of monopile behaviour under cyclic lateral loading", *Proceedings of the 6th International Conference on Offshore Site Investigation and Geotechnics*, *Society for Underwater Technology*, London, UK, pp. 383-390.

Li, M., Zhang, H. and Guan, H. (2011), "Study of offshore monopile behaviour due to ocean waves", *Ocean Eng*., **38**, 1946-1956.

Lin, D.G. and Feng, Z.Y.F. (2006), "A numerical study of piled raft foundations", *J*. *Chinese Inst*. *Eng*., **29**(6), 1091-1097.

Lin, S.S. and Liao, J.C. (1999), "Permanent strains of piles in sand due to cyclic lateral loads", *J*. *Geotech*. *Geoenviron*. *Eng*., *ASCE*, **125**(9), 798-802.

Lin, S., Tseng, Y., Chiang, C. and Hung, C.L. (2005), "Damage of piles caused by lateral spreading – Back study of three cases: Seismic performance and simulation of pile foundations in liquefiable and laterally spreading ground", *ASCE Geotechnical Special Publication*, **145**, 121-133.

Liu, L. and Dobry, R. (1995), *Effect of Liquefaction on Lateral Response of Piles by Centrifuge Model Tests*, NCEER Report to FHWA; *NCEER Bulletin*, **9**(1).

Liyanapathirana, D.S. and Poulos, H.G. (2005), "Seismic lateral response of piles in liquefying soil", *J*. *Geotech*. *Geoenviron*. *Eng*., **131**(12), 1466-1479.

Long, J.H. and Vanneste, G. (1994), "Effects of cyclic lateral loads on piles in sand", *J. Geotech*. *Eng*., *ASCE*, **120**(1), 225-244.

Martin, G.R., Finn, W.D.L. and Seed, H.B. (1975), "Fundamentals of liquefaction under cyclic loading", *J*. *Geotech*. *Eng. Div*., *ASCE*, **101**(5), 423-438.

National Research Council (1985), "Liquefaction of soils during earthquakes", Report No. CETS-EE-001; Committee on Earthquake Engineering, National Academy Press, Washington, D.C., USA.

O'Neill, M.W. and Murchison, J.M. (1983), "An evaluation of *p-y* relationships in sands", Research Report No. GT-DF02-83; University of Houston, Department of Civil Engineering, Houston, TX, USA.
Pacific Earthquake Engineering Research Center (PEER) (2013), Accessed on August 03, 2013 http://peer.berkeley.edu/smcat/search.html
Parker, F. and Reese, L.C. (1970), "*Experimental and Analytical Studies of Behaviour of Single Piles in Sands under Lateral and Axial Loading*", Research Report No. 117-2; University of Texas, Austin, TX, USA.
Pender, M.J. and Pranjoto, S. (1996), "Gapping effects during cyclic lateral loading of piles in clay", *Proceedings of the 11th World Conference on Earthquake Engineering*, Acapulco, Mexico, June.
Popescu, R. and Prevost, J.H. (1993), "Centrifuge validation of a numerical model for dynamic soil liquefaction", *Soil Dyn*. *Earthq*. *Eng*, **12**(2), 73-90.
Reese, L.C., Cox, W.R. and Koop, F.D. (1974), "Analysis of laterally loaded piles in sand", *Proceedings of the 6th Annual Offshore Technology Conference*, Houston, TX, USA, May, Paper No. OTC 2080.
Rollins, K.M., Gerber, T.M., Lane, J.D. and Ashford, S.A. (2005), "Lateral resistance of a full-scale pile group in liquefied sand", *J. Geotech*. *Geoenviron*. *Eng*., *ASCE*, **131**(1), 115-125.
Ryu, C.S. and Yun, C.B. (1992), "Reliability of offshore guyed tower against anchor pile failure", *Eng*. *Struct*., **14**(2), 112-120.
Sanjeev, M. (2011), *Selection*, *Design and Construction of Offshore Wind Turbine Foundations*, In: Wind Turbines, (ISBN 978-953-307-221-0), (Dr. Ibrahim Al-Bahadly Ed.), InTech, Croatia.
Scott, R.F. (1980), "Analysis of Centrifuge Pile", Research Report, OSAPR; American Petrolium Institute, CA, USA.
Sørensen, S.P.H. and Ibsen, L.B. (2013), "Assessment of foundation design for offshore monopiles unprotected against scour", *Ocean Eng*., **63**, 17-25.
Taşan, H.E., Rackwitz, F. and Savidis, S.A. (2010), "Behaviour of cyclic laterally loaded large diameter monopiles in saturated sand", *Proceedings of 7th European Conference on Numerical Methods in Geotechnical Engineering*, Trondheim, Norway, June, pp. 889-894.
Tokimatsu, K. and Asaka, Y. (1998), "Effects of liquefaction-displacements on pile performance in the 1995 Hyogeken- Nambu earthquake", *Soil*. *Found*. (Special Issue), 163-177.
Tokimatsu, K., Mizuno, H. and Kakurai, M. (1996), "Building damage associated with geotechnical problems", *Soil*. *Found*. (Special Issue), 219-234.
Tokimatsu, K. (1999), "Performance of pile foundations in laterally spreading soils", *Proceedings of the 2nd International Conference on Earthquake Geotechnical Engineering*, Lisbon, Portugal, June, pp. 957-964.
Wang, J.L., Yan, S.W. and Huo, Z.L. (2013a), "Failure mode of monopile foundation for offshore wind turbines under monotonic loading", *Appl*. *Mech*. *Mater*., **256-259**, 1071-1074.
Wang, J.L., Yan, S.W. and Huo, Z.L. (2013b), "Study of Failure Patterns of Monopile Foundation for Offshore Wind Turbines under Combined Loading", Site Investigation Science and Technology.
Wilson, D.W., Boulanger, R.W. and Kutter, B.L. (2000), "Observed seismic lateral resistance of liquefying sand", *J. Geotech*. *Geoenviron*. *Eng*. *ASCE*, **126**(10), 898-906.
Wilson, D.W., Boulanger, R.W. and Kutter, B.L. (2000), "Observed seismic lateral resistance of liquefying sand", *J. Geotech*. *Geoenviron*. *Eng*., *ASCE*, **126**(10), 898-906.
Yasuda, S., Yoshida, N., Kiku, H., Adachi, K. and Gose, S. (1999), *A Simplified Method to Evaluate Liquefaction-Induced Deformation*, (ISBN 90-5809-1163), Earthquake Geotechnical Engineering, Balkema, Rotterdam, Netherlands.
Zafeirakos, A. and Gerolymos, N. (2013), "On the seismic response of under-designed caisson foundations", *Bull Earthq*. *Eng*., **11**(5), 1337-1372.
Zienkiewicz, O.C., Chan, A.H.C., Pastor, M., Schrefler, B.A. and Shiomi, T. (1999), *Computatioal Geomechanics with Special Reference to Earthquake Engineering*, John Wiley & Sons Ltd., England.

CC

Nomenclature

k_s	The shear stiffness for interface
k_n	The normal stiffness for interface
$\Delta Z_{\min}$	Minimum zone size in vertical direction
K	Bulk modulus
G	Shear modulus
ϕ	Friction angle
K_w	Bulk modulus of water
$(N_1)_{60}$	Normalized SPT-N value
F_A	Maximum soil flow pressure (at point A)
F_B	Maximum soil flow pressure (at point B)
$a_{\max,base}$ (g)	Peak acceleration value